Implementation of the COST 273 Directional Channel Model in Microcell Scenarios

Ivo Sousa, Maria Paula Queluz and António Rodrigues
Instituto de Telecomunicações/Instituto Superior Técnico, Technical University of Lisbon, Lisbon, Portugal

Keywords: COST 273 Directional Channel Model, Microcells, Wireless Communications.

Abstract: This paper presents a tutorial on how to implement the COST 273 Directional Channel Model (DCM) for microcell scenarios. Special care has been taken to present all the parameters models and values required by the DCM, being some of them proposed in this work because they were missing in the related literature and are essential. The results and comparison with experimental data of an implementation example are also presented, which prove that this DCM is suitable for wireless systems development, especially those that exploit spatial aspects of radio channels, like for example Multiple-Input Multiple-Output (MIMO) systems.

1 INTRODUCTION

Wireless communication systems can be implemented with multiple antennas at the transmitter and at the receiver, in order to exploit spatial differences of a radio channel. These systems, commonly known as Multiple-Input Multiple-Output (MIMO) systems, allow to improve the spectral efficiency by offering a spatial multiplexing gain, or allow to improve the link reliability by offering a diversity gain (Foschini and Gans, 1998; Telatar, 1999). These gains are achieved without increased transmit power or additional bandwidth, which is MIMO systems major advantage.

For a correct MIMO system development it is important to understand and characterize the propagation phenomena between Base Stations (BSs) and Mobile Stations (MSs). This phenomena depends not only on the wavelength and distance between BSs and MSs, but also on all the Interacting Objects (IOs) present in the surrounding environment where waves bounce. These IOs are designated as scatterers since they induce scattering, where one or more non-uniformities in the medium force radio waves to deviate from a straight trajectory. To properly simulate the radio wave propagation and incorporate realistic features, like time-variant characteristics, frequency selective responses and correct spatial representation of the scenarios, Directional Channel Models (DCMs) have been developed, which aim to be easy-to-use methods in order to avoid extensive measurement campaigns. A survey about DCMs classification can be found in (Almers et al., 2007).

The aim of this paper is to provide a tutorial on the COST 273 DCM implementation for microcells. All parameters models and values required by the DCM are presented, including some that had to be empirically defined because they were missing in the literature and are essential. Following this introduction, Section 2 describes the COST 273 DCM applied to microcells. An implementation example is presented in section 3, followed by final remarks in section 4.

2 COST 273 DCM – MICROCELLS

COST is an intergovernmental framework for European Cooperation in Science and Technology, allowing a European coordination of nationally-funded research. DCMs were developed within the Information and Communication Technologies COST domain.

The COST 273 DCM (Correia, 2006) is a general model, since it is defined for several radio environments and uses an identical generic model for all cell types (macro-, micro- and picocells). This DCM is the successor of the COST 259 DCM (Correia, 2001), being the main update a more realistic modeling of the multiple-bounce scattering effect (especially important for micro- and picocell scenarios simulations). The latest COST DCM is the COST 2100 DCM (Verdone and Zanella, 2012), but since this DCM is very recent, it is not yet fully parametrized, fully implemented and widely used (for example, parameters for outdoor scenarios remain important missing parts).

Sousa I., Paula Queluz M. and Rodrigues A..
Implementation of the COST 273 Directional Channel Model in Microcell Scenarios.
DOI: 10.5220/0004058303490356
In *Proceedings of the International Conference on Signal Processing and Multimedia Applications and Wireless Information Networks and Systems* (WINSYS-2012), pages 349-356
ISBN: 978-989-8565-25-9

Table 1: External parameters.

Parameter	Symbol	Validity range
Carrier freq. [GHz]	f_c	1–5
BS/MS height [m]	h_{BS}/h_{MS}	3–10/1.5
BS/MS position [m]	$\vec{r}_{BS}/\vec{r}_{MS}$	(0,0,h_{BS})/Any
Cell radius [m]	R_{cell}	Any

2.1 Model General Structure

The COST 273 DCM follows an approach where physical positions of the transmitter, receiver, scatterers and their effect on the electromagnetic waves are defined so that the Double-Directional Channel Impulse Response (DDCIR) is obtained as a superposition of MultiPath Components (MPCs). In other words, the DDCIR is given by (Molisch et al., 2006)

$$\underline{h}(t,\tau,\Omega,\Psi) = \sum_{l=1}^{L(\vec{r})} \underline{a}_l \delta(\tau-\tau_l)\,\delta(\Omega-\Omega_l)\,\delta(\Psi-\Psi_l) \quad (1)$$

where t is the absolute time, τ is the delay variable, Ω and Ψ are spatial angles characterizing the MPCs' Direction of Arrival (DoA) and Direction of Departure (DoD), respectively, $\vec{r}$ denotes the location of the receiver antenna with respect to the transmitter antenna, $\underline{a}_l$ represents the l^{th} MPC complex amplitude (polarimetric 2×2 matrix) and $\delta(\cdot)$ is the Dirac delta function.

The description of the DDCIR in (1) is antenna independent. The non-directional time-variant Channel Impulse Response (CIR) can be obtained by integrating over the DoDs and DoAs weighted by the transmitter and receiver complex polarimetric antenna gains $\vec{G}_T(\Psi)$ and $\vec{G}_R(\Omega)$, respectively, i.e.,

$$h(t,\tau) = \int_{\Psi}\int_{\Omega} \underline{h}(t,\tau,\Omega,\Psi)\,\vec{G}_T(\Psi)\vec{G}_R(\Omega)\,d\Omega\,d\Psi \quad (2)$$

2.2 Parameters Models and Settings

2.2.1 External Parameters

Table 1 presents the external parameters required by the COST 273 DCM for microcells (Correia, 2006), which are user-supplied but have validity ranges.

The COST 273 DCM uses as path-loss model for microcells the same one as the COST 259 DCM, which is described in (Feuerstein et al., 1994) as a one- or two-slope log-distance law, depending on whether there is Line-of-Sight (LoS) or not (NLoS):

$$L_{p,\mathrm{LoS}}(d) = \begin{cases} 10n_1\log_{10}(d) \\ \quad +L_0(1\mathrm{m}) \quad [\mathrm{dB}] \quad \text{if } 1<d<d_f \\ 10n_2\log_{10}(d/d_f)+10n_1\log_{10}(d_f) \\ \quad +L_0(1\mathrm{m}) \quad [\mathrm{dB}] \quad \text{if } d>d_f \end{cases}$$

Table 2: Path-loss coefficients (for 2 GHz).

Coefficient	Value
$n_1/n_2/n_3$	2.2/3.3/2.6

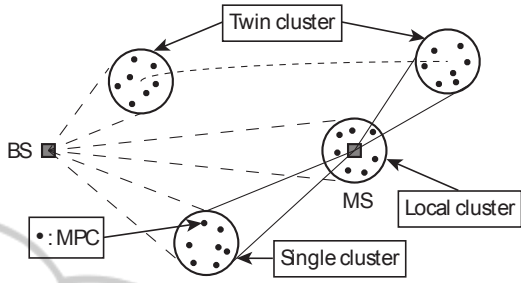

Figure 1: General description of the COST 273 DCM.

$$L_{p,\mathrm{NLoS}}(d) = 10n_3\log_{10}(d)+L_0(1\mathrm{m}) \quad [\mathrm{dB}]$$
$$L_0(1\mathrm{m}) = 20\log_{10}(4\pi(1\mathrm{m})/\lambda) \quad [\mathrm{dB}] \quad (3)$$

where d is the distance between the BS and the MS, λ denotes the wavelength ($\lambda = c_0/f_c$, being c_0 the speed of light) and the breakpoint value d_f is given by

$$d_f = \frac{1}{\lambda}\sqrt{(\Gamma^2-\Lambda^2)^2 - 2(\Gamma^2+\Lambda^2)\left(\frac{\lambda}{2}\right)^2 + \left(\frac{\lambda}{2}\right)^4} \quad (4)$$

with $\Gamma = h_{BS}+h_{MS}$ and $\Lambda = h_{BS}-h_{MS}$. The values of the empirical regression coefficients n_1, n_2 and n_3 for 2 GHz are given in Table 2 (Correia, 2001).

2.2.2 Clusters General Considerations

In the COST 273 DCM first the scatterers are stochastically distributed in the physical environment and then the corresponding MPCs are computed using a simple ray tracing technique. Each MPC is characterized by its delay and angles (azimuth and elevation). Since there are MPCs with similar delay and angles, they can be grouped into a cluster, which enables the use of less parameters to describe the channel.

As Figure 1 shows, three kinds of clusters are used in this DCM: *local clusters*, *single-interaction clusters* and *twin clusters*. Local and single-interaction clusters account for single-bounce scatterers, while twin clusters allow to simulate the multiple-bounce behavior. For microcells, there is an equal number of single and twin clusters (Correia, 2006).

2.2.3 Number of Clusters and Visibility Region

Many clusters can exist in the radio environment but only some are active, meaning that only those contribute to the CIR. The Visibility Region (VR) concept

Table 3: Visibility region parameters.

Parameter	Value
N_C/R_C [m]/L_C [m]	4/50/20

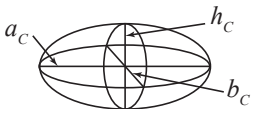

Figure 2: Clusters geometry.

is used to determine whether or not a cluster is active, where each VR is associated with only one cluster: if the MS is in a VR, then the corresponding cluster is active; otherwise the cluster is non-active. VRs are circular regions with identical size on the *xy* plane. The relative power of the cluster m associated to a certain VR is scaled by a factor A_m^2, with A_m given by

$$A_m(\vec{r}_{MS}) = \frac{1}{2} - \frac{1}{\pi}\arctan\left(\frac{2\sqrt{2}(L_C + d_{MS,VR} - R_C)}{\sqrt{\lambda L_C}}\right) \quad (5)$$

where R_C is the VR radius, L_C is the size of the transition region and $d_{MS,VR}$ is the distance between the MS and the VR center. For an expected number of active clusters equal to N_C, the VRs area density needs to be

$$\rho_C = (N_C - 1)\,/\,\left(\pi(R_C - L_C)^2\right)\,[\mathrm{m}^{-2}] \quad (6)$$

where the $N_C - 1$ term comes from the fact that there is always an active cluster around a MS, i.e., $A_1 = 1$. The VRs are uniformly distributed in the simulation environment. Table 3 presents the values of N_C, R_C and L_C for microcells (Correia, 2006).

2.2.4 Local Clusters Generation

One cluster is always present around a MS and it is always active. It is named local cluster since its center is co-located with the MS. This cluster contains single-bounce MPCs that introduce a large azimuth spread with low delay at the MS.

All kinds of clusters can be seen as ellipsoids in space, each one characterized by the extents in space a_C, b_C and h_C, Figure 2. In the model implementation, a local cluster is assumed to be circular in the *xy* plane, i.e., the ground plane ($a_C = b_C$), being its spatial spread only determined by its delay spread (a_C) and elevation spread (h_C). The computation of these spreads, along with the MPCs positioning within the cluster, will be seen later on.

2.2.5 Single-interaction Clusters Generation

The positioning of a single-interaction cluster is obtained using a simple geometric approach. First an imaginary line is drawn from the BS to the center of the VR associated with the cluster, then the azimuth angle between this line and the cluster is obtained from a Gaussian distribution with a standard deviation $\sigma_{\phi,C}$. The distance in the *xy* plane from the BS to the cluster is given by the exponential distribution

$$f_{r_C}(r_C) = \begin{cases} 0 & \text{if } r_C < r_{\min} \\ \frac{1}{\sigma_{r,C}} e^{-(r_C - r_{\min})/\sigma_{r,C}} & \text{if } r_C \geq r_{\min} \end{cases} \quad (7)$$

The values for $r_{\min}$, $\sigma_{r,C}$ and $\sigma_{\phi,C}$ are presented in Table 4. They were empirically chosen since values for microcell scenarios were not found in the literature. The proposed $\sigma_{r,C}$ value guarantees that the distance r_C is less than or equal to 150 m in 95% of the times.

The above procedure only fixes the position of the cluster in the *xy* plane. The COST 273 DCM does not suggest any approach for the cluster height, so for the model implementation an uniform distribution between the ground and the BS height is proposed.

The spatial spread (Figure 2) of single-interaction clusters is determined by its delay, azimuth and elevation spread (a_C, b_C and h_C, respectively).

Table 4: Single-interaction clusters position parameters.

Parameter	Value
$r_{\min}$ [m]/$\sigma_{r,C}$ [m]/$\sigma_{\phi,C}$ [deg]	5/48.4/22.5

Table 5: Twin clusters position parameters.

Parameter	Value [deg]
ζ_{BS}/ζ_{MS}	22.5/180

2.2.6 Twin Clusters Generation

Twin clusters are represented by two clusters with the same IOs distribution and number, corresponding one cluster to the BS side and the other to the MS side. This representation allows independent modeling of the angular dispersion at the BS and at the MS. First, the azimuth of a cluster seen from the BS (MS) side is computed from an uniform distribution within the interval $[-\zeta_{BS}, +\zeta_{BS}]$ ($[-\zeta_{MS}, +\zeta_{MS}]$), where the angle 0 represents the imaginary line from the BS to the center of the VR associated with the twin cluster. These parameters values are given in Table 5 (Correia, 2006). The distance in the *xy* plane from the cluster to the BS (VR center where the MS is) is given by

$$d_{BS/MS} = (\Delta\tau\, c_0)\,/\,\left(4\tan\varphi_{BS/MS}\right) \quad (8)$$

being $\Delta\tau$ and φ_{BS} (φ_{MS}) the delay and azimuth spread seen from the BS (MS), respectively.

Again, this procedure only fixes the *xy* plane position of the cluster. Like the single-interaction clusters case, we propose an uniform distribution between the

Table 6: Cluster spread parameters.

Parameter	Value
μ_τ [ns]/σ_τ [dB]/σ_S [dB]	13/14/2.9
$\mu_{\varphi_{BS}}$ [deg]/$\mu_{\varphi_{MS}}$ [deg]	2.3/2.3
$\sigma_{\varphi_{BS}}$ [dB]/$\sigma_{\varphi_{MS}}$ [dB]	3.4/3.4
$\mu_{\theta_{BS}}$ [deg]/$\mu_{\theta_{MS}}$ [deg]	1.3/1.3
$\sigma_{\theta_{BS}}$ [dB]/$\sigma_{\theta_{MS}}$ [dB]	3.3/3.3

ground and the BS height (independent for each of the two representations) for model implementation.

The two representations of a twin cluster have the same delay spread, being it circular in the *xy* plane ($a_C = b_C$), while each representation (BS and MS) sees a different elevation spread ($h_{C,BS}$ and $h_{C,MS}$).

2.2.7 Clusters Dispersion

For any type of clusters, the delay spread, angular spreads and shadow fading of a cluster *m* are correlated random variables, given respectively by

$$\Delta\tau_m = \mu_\tau (d/1000)^{0.5}\, 10^{\sigma_\tau Z_m/10} \quad (9)$$

$$\beta_m = \mu_\beta 10^{\sigma_\beta Y_m/10} \quad (10)$$

$$S_m = 10^{\sigma_S X_m/10} \quad (11)$$

where Z_m, Y_m and X_m are correlated Gaussian random variables, with zero mean and unit variance, and β represents one of the angular spreads, i.e., azimuth or elevation spread for the BS side (φ_{BS} or θ_{BS}) or for the MS side (φ_{MS} or θ_{MS}). The parameters values needed to compute a cluster spread are presented in Table 6 (Correia, 2006). The correlated random processes can be computed using the Cholesky factorization, characterized by the cross-correlation coefficients given in Table 7 (Correia, 2006). After computing the spreads of a cluster, its ellipsoid (Figure 2) can then be characterized. The delay spread dimension is given by

$$d_\tau = \Delta\tau c_0/2 \quad (12)$$

while the azimuth ($\beta = \varphi_{BS/MS}$) and elevation ($\beta = \theta_{BS/MS}$) spreads dimensions are given by

$$d_\beta = d_{C,BS/MS} \tan\beta \quad (13)$$

where $d_{C,BS}$ ($d_{C,MS}$) is the distance between the cluster and the BS (VR center where the MS is). Table 8 summarizes the clusters spatial characterization.

2.2.8 IOs Positioning

The COST 273 DCM uses for microcells 7 MPCs per cluster. The positioning of the IOs (each IO corresponds to one MPC) differs if they represent single-bounce scatterers (local and single-interaction clusters) or multiple-bounce scatterers (twin clusters).

Table 7: Cross-correlation coefficients.

Coefficient	Value
$\rho_{\tau-\varphi_{BS}}/\rho_{\tau-\varphi_{MS}}/\rho_{\tau-S}$	0.1/0.1/0.04
$\rho_{\varphi_{BS}-S}/\rho_{\varphi_{MS}-S}$/ all other	$-0.2/-0.2/0$

Table 8: Cluster spatial spread.

Type	a_C	b_C	h_C
Local	$\Delta\tau c_0/2$	$= a_C$	$d_{C,BS}\tan\theta_{BS}$
Single	$\Delta\tau c_0/2$	$d_{C,BS}\tan\varphi_{BS}$	$d_{C,BS}\tan\theta_{BS}$
T. (BS)	$\Delta\tau c_0/2$	$= a_C$	$d_{C,BS}\tan\theta_{BS}$
T. (MS)	=Twin (BS)		$d_{C,MS}\tan\theta_{MS}$

For single-bounce scatterers, the distance between the cluster center and an IO is based on the truncated one-sided Gaussian distribution (Laurila et al., 1998)

$$f_{r_{IO}}(r_{IO}) = \begin{cases} \frac{1}{\sqrt{2\pi}} e^{-r^2/2} & \text{if } 0 \le r_{IO} \le r_T \\ 0 & \text{otherwise} \end{cases} \quad (14)$$

where $r_T = 3$ (Correia, 2006). Uniform distributions are assumed for the azimuth (φ_{IO}) and elevation (θ_{IO}) directions. The relative position of an IO with respect to the cluster center is obtained by computing r_{IO}, φ_{IO} and θ_{IO}, followed by a conversion to a Cartesian coordinate system (*xyz*); after that, these values (x_{IO}, y_{IO} and z_{IO}) are multiplied by the cluster ellipsoid spatial spread (a_C, b_C and h_C from Table 8).

For twin clusters, the COST 273 DCM uses an IO distribution in all dimensions based on the truncated Gaussian distribution (shown here for one dimension)

$$f_{x_{IO}}(x_{IO}) = \begin{cases} \frac{1}{\sqrt{2\pi}} e^{-x_{IO}^2/2} & \text{if } |x_{IO}| \le x_T \\ 0 & \text{if } |x_{IO}| > x_T \end{cases} \quad (15)$$

where $x_T = 3$ (Correia, 2006). The relative position of an IO is obtained as follows: first x_{IO}, y_{IO} and z_{IO} are computed using (15) (these random generated values are used for both representations of the twin cluster – BS side and MS side – to guarantee consistent delay and angular spreads); then they are multiplied by the cluster spatial spread (a_C, b_C and h_C from Table 8).

To match the spatial spread with the delay and angular spreads viewed from the BS (VR center where the MS is, for the MS side representation of twin clusters), clusters are rotated in order to become oriented towards the BS (away from the MS, for the MS side representation of twin clusters). This rotation is attained by multiplying the previously computed IOs relative positions by the following rotation matrix

$$\begin{pmatrix} \cos\Phi\cos\Theta & -\sin\Phi & \cos\Phi\sin\Theta \\ \sin\Phi\cos\Theta & \cos\Phi & \sin\Phi\sin\Theta \\ -\sin\Theta & 0 & \cos\Theta \end{pmatrix} \quad (16)$$

Table 9: MPCs power parameters.

Parameter	Value
k_τ [dB/μs]/τ_B [μs]	40/0.5
K_{MPC} [dB]/μ_K/σ_K	2/7/2.3

where $(\Phi,\Theta) = (\Phi_{BS},\Theta_{BS})$, being Φ_{BS} and Θ_{BS} the azimuth and elevation angles of the cluster seen from the BS (for the MS side representation of twin clusters $(\Phi,\Theta) = (\Phi_{MS}+\pi,\Theta_{MS}+\pi)$, being Φ_{MS} and Θ_{MS} the azimuth and elevation angles of the cluster seen from the VR center where a MS is).

2.2.9 MPCs Power

The COST 273 DCM assumes that the power attenuation of a cluster m is a function of its delay (τ_m) with respect to the LoS delay (τ_0), i.e., the longer the delay, the smaller is the power that the cluster carries. Hence, the power attenuation of a cluster is given by

$$P_m = \max\left\{e^{-k_\tau(\tau_m-\tau_0)}, e^{-k_\tau(\tau_B-\tau_0)}\right\} \quad (17)$$

where k_τ is the decaying parameter and τ_B is the cut-off delay. The delay of a cluster is given by

$$\tau_m = (d_{C_m,BS} + d_{C_m,MS})/c_0 + \tau_{C_m,link} \quad (18)$$

where $\tau_{C_m,link}$ is either the cluster-link delay between the two representation of twin clusters (computed using a similar geometric relationship) or assumes $\tau_{C,link} = 0$ for local and single-interaction clusters.

The power P_{MPC} of each MPCs within a cluster is characterized through a Ricean distribution

$$f_{\text{Rice}}(w) = \frac{w}{\sigma_K^2} I_0\left(\frac{wA_K}{\sigma_K^2}\right) e^{-(w^2+A_K^2)/(2\sigma_K^2)} \quad (19)$$

where $I_0(\cdot)$ denotes the modified Bessel function of the first kind with order zero, and the Rice factor K_{MPC} is related to the parameters A_K and σ_K by

$$K_{MPC} = A_K^2/(2\sigma_K^2) \quad (20)$$

The complex amplitude of the MPC l in the cluster m is given by (for one polarization component)

$$a_{m,l} = \sqrt{L_p A_m^2 S_m P_m P_{MPC,m,l}}\, e^{-j2\pi f_c \tau_{m,l}} \quad (21)$$

where $\tau_{m,l}$ is the delay of the MPC given by

$$\tau_{m,l} = (d_{MPC_{m,l},BS} + d_{MPC_{m,l},MS})/c_0 + \tau_{C_m,link} \quad (22)$$

For LoS situations the DDCIR has an extra MPC

$$a_{LoS} = \sqrt{L_p P_{LoS}}\, e^{-j2\pi f_c \tau_0} \quad (23)$$

where P_{LoS} is the LoS power factor drawn from a log-normal distribution with mean μ_K and standard deviation σ_K. The values of the parameters introduced in this subsection are given in Table 9 (Correia, 2006).

Table 10: Polarization coefficients relations.

Parameter	Value [dB]
$\mu_{\text{XPD}}/\mu_{\text{VV/HH}}/\mu_{\text{VH/HV}}$	8.5/0.3/−0.5
$\sigma_{\text{XPD}}/\sigma_{\text{VV/HH}}/\sigma_{\text{VH/HV}}$	1.8/3.2/1.8

Table 11: Autocorrelation distances.

Parameter	Value [m]
$L_S/L_\tau/L_{\varphi_{BS}}/L_{\theta_{BS}}/L_{\varphi_{MS}}/L_{\theta_{MS}}$	5/5/50/50/25/25

2.2.10 Polarization

The polarization is characterized by the matrix

$$\begin{pmatrix} P_{VV} & P_{VH} \\ P_{HV} & P_{HH} \end{pmatrix} \quad (24)$$

where the entries characterize the powers of each polarization component. The ratio

$$\text{XPD} = (P_{VV}+P_{HH})/(P_{VH}+P_{HV}) \quad (25)$$

is log-normally distributed, with mean μ_{XPD} and standard deviation σ_{XPD}. Other relations between the polarization coefficients are also modeled log-normally with the values presented in Table 10 (Correia, 2006).

2.2.11 Other Considerations

The COST 273 DCM described previously is envisioned for singe-link scenarios, i.e., where only one BS and one MS are present. In order to study the correlation between different links, one can extend the model to multi-MS scenarios by dropping multiple MSs into the simulation environment and use the same VRs and corresponding clusters for each MS.

The MSs positional data can be given by any mobility model. When introducing movement, the shadowing as well as the delay and angular spreads are characterized by the spatial autocorrelation function

$$ACF(x,x') = e^{-|x-x'|/L_x} \quad (26)$$

with the respective autocorrelation distances L_x shown in Table 11 (Correia, 2006).

Another important aspect of the model's implementation is the simulation area, i.e., the area where the MSs can be and where the VRs are (the corresponding clusters can be anywhere since they are stochastically determined). Since the clusters attenuation power given by (17) should not be greater than one, the MSs should not be separated from the BS by more than $\tau_B \times c_0 = 150$ m (Table 9). Recalling that the VRs are uniformly distributed in the simulation area, this simulation area should be at least extended by the radius of the VRs (from Table 3, $R_C = 50$ m)

from the farthest MS away from the BS. This avoids effects introduced by the simulation area limits.

Since one spatial dimension of any cluster is always characterized by its delay spread, the stochastic generation of this parameter can yield a large unrealistic cluster size. To avoid this situation, a maximum value for the delay spread of 120 ns (Correia, 2001) should be applied when using expression (9).

3 IMPLEMENTATION EXAMPLE

Validation of a channel model simulator is very important to ensure that the outputs are realistic and can be used for MIMO systems development, for example. To this end, a large number of channel realizations were generated using a multi-MS scenario simulator developed in MATLAB® based on the COST 273 DCM described previously. Those results were then compared with measurements available in the literature. This procedure allows not only to validate if the different sub-models for cluster and MPC behavior are well combined, but it also allows to infer if the values used for cluster positioning that were proposed in this work are adequate.

3.1 Simulation Parameters

The test environment is characterized by a BS (10 m height) located in the center of a 100 m $\times$ 100 m microcell. MSs (1.5 m height) are evenly positioned in the microcell, being separated between them by 1 m, which makes a total of 10201 MSs. An operating frequency of 2 GHz is used and the VRs can be in a 200 m $\times$ 200 m area (center co-located with the BS), in order to avoid simulation area limits effects.

Each simulation run has a different distribution of VRs and different stochastic parameters, hence corresponds to a different radio channel situation. Also, no mobility model is used, so each run represents a snapshot of the radio environment.

3.2 Simulation Results

The following simulation results are based on 200 simulations runs. Table 12 presents the environment characterization related with measurements values available in the literature. The indicated references correspond to: [1]-present simulator; [2]-(Kozono and Taguchi, 1993); [3]-(Devasirvatham, 1988); [4]-(Zhao et al., 2002); [5]-(3GPP, 2011); [6]-(Pajusco, 1998); [7]-(Correia, 2006).

Table 12: Reference scenarios.

Reference	R_{cell} [m]	f_c [GHz]	h_{BS}/h_{MS} [m]
[1]	71	2	$10/1.5$
[2]	1000	1.5	$5/1.5$
[3]	150	0.85	$9.1/1.8$
[4]	200	5.3	$12/2$
[5]	500	1.9	$12.5/1.5$
[6]	300	2.2	$7/*$
[7]	†	5.3	‡/$*$

† – only info available is that it is a microcell environment

‡ – only info available is that BS antenna is on rooftop

$*$ – only info available is that MSs are on the street

Table 13: Delay spread comparison.

Statistical measure	Delay spread [ns]			
	[1]	[2]	[3]	[4]
median – LoS	6	—	30	31
median – NLoS	14	—	50	—
maximum – LoS	68	250	62	64
maximum – NLoS	297	300	330	—

3.2.1 Delay Spread

The delay spread can be used as a measure of the multipath propagation phenomenon. Given measured delay profiles, the delay spread is calculated using the formula presented in (Kozono and Taguchi, 1993).

Table 13 presents some delay spread values obtained by the simulator along with measurements values available in the literature. The simulated values generally agree with experimental data, especially when considering the maximum delay spread case. Also, simulated delay spread values are lower for the LoS case. This is an expected result, also verified by the measurements, due to the fact that the LoS component has associated a higher power when compared to the other MPCs, thus leading to a lower delay spread value. The median values obtained by simulation are lower than the ones measured, which could mean a lower multipath richness. Since lower multipath richness usually means lower MIMO gain (MIMO channels become more correlated), one could say that this implementation simulates a worst case scenario.

3.2.2 Azimuth Spread

The computation of the angular spread is performed as mentioned in (3GPP, 2011), which is somewhat similar to the delay spread computation but takes into account the ambiguity of the modulo 2π operation.

Table 14 presents some azimuth spread values obtained by the simulator along with measurements values available in the literature. Once again, the val-

Table 14: Azimuth spread comparison.

Statistical measure	Azimuth spread [deg]			
	[1]	[5]	[6]	[7]
median – BS, LoS	3.7	5.0	7.5	5.1
median – MS, LoS	30.8	62.5	—	28.9
median – BS, NLoS	9.4	19.0	20.0	12.6
median – MS, NLoS	73.3	68.0	—	40.3

Table 15: Elevation spread comparison.

Statistical measure	Elevation spread [deg]	
	[1]	[7]
median – BS, LoS	3.3	1.3
median – MS, LoS	18.4	2.5
median – BS, NLoS	8.3	2.5
median – MS, NLoS	48.4	4.7

ues obtained by the simulator generally agree with the measurements available in the literature. As can be seen, azimuth spread values are lower for the LoS cases. This result is again expected for the same reasons as in the delay spread case, and once more it is verified by the experimental data. Also, the simulated azimuth spread is higher at the MSs than at the BS, which is consistent with the measurements. This can be justified by the always existent local cluster around a MS and the use of the twin cluster concept.

3.2.3 Elevation Spread

Unlike the previous case, there is no modulo 2π operation ambiguity when computing the elevation spread, so an equivalent formula of the delay spread is used.

Table 15 presents some elevation spread values obtained by the simulator along with measurements values available in the literature. In this case, the simulated values do not agree quantitatively with the experimental data from the only reference available. Besides the fact that the reference scenario physical characteristics are not fully know and might be a lot different, also the influence of the antennas' operational angular ranges was not taken into account in the measurements, as stated in (Correia, 2006). This could mean a reduction in the elevation spread if the measurement antennas were not omnidirectional in the elevation plane. From a qualitative point of view, the simulated results agree with the experimental data, because elevation spread values are lower for the LoS case for both spreads observed at the BS and at the MSs; also, the elevation spread generated by the simulator is higher at the MSs than at the BS.

4 FINAL REMARKS

This paper presents a tutorial on how to implement the COST 273 DCM for microcell scenarios. All parameters models and values required by the DCM that were disperse in the literature are gathered in this work, as well as some values that were proposed here, because they were missing in the literature and are essential. An implementation example of this COST 273 DCM proved that its results agree with experimental data, hence it is suitable for MIMO systems development.

ACKNOWLEDGEMENTS

This work was partially funded by Instituto de Telecomunicações/LA and by Fundação para a Ciência e a Tecnologia (FCT) under a Doctoral grant (SFRH/BD/62003/2009).

REFERENCES

3GPP (2011). Spatial Channel Model for Multiple Input Multiple Output (MIMO) Simulations. Technical Report 25.996, v. 10.0.0. www.3gpp.org/specifications.

Almers, P., Bonek, E., Burr, A., et al. (2007). Survey of Channel and Radio Propagation Models for Wireless MIMO Systems. *EURASIP Journal on Wireless Communications and Networking*, 2007.

Correia, L. (2001). *Wireless Flexible Personalized Communications, COST 259: European Co-operation in Mobile Radio Research*. John Wiley & Sons, Inc.

Correia, L. (2006). *Mobile Broadband Multimedia Networks: Techniques, Models and Tools for 4G*. Academic Press.

Devasirvatham, D. (1988). Radio Propagation Studies in a Small City for Universal Portable Communications. In *IEEE 38th VTC*, pages 100–104.

Feuerstein, M., Blackard, K., et al. (1994). Path Loss, Delay Spread, and Outage Models as Functions of Antenna Height for Microcellular System Design. *IEEE Transactions on Vehicular Technology*, 43(3):487–498.

Foschini, G. and Gans, M. (1998). On Limits of Wireless Communications in a Fading Environment when Using Multiple Antennas. *Wireless Personal Communications*, 6:311–335.

Kozono, S. and Taguchi, A. (1993). Mobile Propagation Loss and Delay Spread Characteristics with a Low Base Station Antenna on an Urban Road. *IEEE Transactions on Vehicular Technology*, 42(1):103–109.

Laurila, J., Molisch, A., and Bonek, E. (1998). Influence of the Scatterer Distribution on Power Delay Profiles and Azimuthal Power Spectra of Mobile Radio Channels. In *IEEE 5th ISSSTA*, volume 1, pages 267–271.

Molisch, A., Asplund, H., et al. (2006). The COST259 Directional Channel Model–Part I: Overview and

Methodology. *IEEE Transactions on Wireless Communications*, 5(12):3421–3433.

Pajusco, P. (1998). Experimental Characterization of DOA at the Base Station in Rural and Urban Area. In *IEEE 48th VTC*, volume 2, pages 993–997.

Telatar, E. (1999). Capacity of Multi-antenna Gaussian Channels. *European Transactions on Telecommunications*, 10:585–595.

Verdone, R. and Zanella, A. (2012). *Pervasive Mobile and Ambient Wireless Communications: COST Action 2100*. Springer.

Zhao, X., Kivinen, J., Vainikainen, P., and Skog, K. (2002). Propagation Characteristics for Wideband Outdoor Mobile Communications at 5.3 GHz. *IEEE Journal on Selected Areas in Communications*, 20(3):507–514.